Simultaneous Extrapolation in Time and Frequency Domains Using Hermite Expansions

Murli Mohan Rao, Tapan K. Sarkar, *Fellow, IEEE*, Tricha Anjali, and Raviraj S. Adve

Abstract— The time-domain response of a three-dimensional (3-D) conducting object is modeled as an associate hermite (AH) series expansion. Using the isomorphism of the AH function and its Fourier transform, the frequency-domain response can be expressed as a *scaled* version of the time-domain expansion. Using early-time and low-frequency data, we demonstrate simultaneous expansion in both domains. This approach is attractive because expansions with only 10–20 terms give good extrapolation in both time and frequency domains. The computation involved is minimal with this method.

Index Terms— Frequency-domain analysis, time-domain analysis.

I. INTRODUCTION

IN electromagnetic analysis, field quantities are usually assumed to be time harmonic. This suggests that the solution lies in the frequency domain. The method of moments (MoM), which uses an integral equation formulation, can be used to perform the frequency-domain analysis. However, for broadband analysis, this approach can get computationally very intensive; as the MoM program needs to be executed for each frequency of interest and for high frequencies, the size of the matrix can be very large.

The time-domain approach is prefered for broad-band analysis. Other advantages of a time-domain formulation include easier modeling of nonlinear and time-varying media and use of gating to eliminate unwanted reflections. For a time-domain integral equation formulation, the method of marching on in time (MoT) is usually employed. A serious drawback of this algorithm is the occurance of late-time instabilities in the form of high-frequency oscillations [1].

In this paper, we present a technique to overcome the late-time oscillations. Using early-time and low-frequency data, we obtain stable late-time and broad-band information. The MoM approach can efficiently generate low frequency data, while the MoT algorithm can be used to obtain stable early-time data quickly. The overall analysis is thus computationally very efficient.

The time- and frequency-domain responses of three-dimensional (3-D) conducting objects are considered in this paper. It is assumed that the conducting structures are excited by band-limited functions such that both the time- and frequency-domain responses are of finite support for all practical purposes. The energy content of the response is almost entirely concentrated in a finite portion of the time and frequency axes.

For these responses, an optimal choice of basis functions would, therefore, be one that provides compact support. The associate hermite (AH) series is well suited for signals with compact support [2]. The isomorphism between the AH function and its Fourier transform allows us to work simultaneously with time- and frequency-domain data.

In the next section, we introduce the AH functions and set up the matrix equation of the problem. In Section III we discuss some numerical results. Finally, some conclusions are presented in Section IV.

II. FORMULATION

Consider the set of functions [2]

$$h_n(t, l) = \frac{H_n\left(\frac{t}{l}\right)}{\sqrt{2^n n!}} \frac{e^{\frac{-t^2}{2l^2}}}{\sqrt{\sqrt{\pi} l}}, \qquad n \geq 0 \qquad (1)$$

where $H_n(t)$ is the hermite polynomial of order n, with l as a scaling factor and $n!$ represents factorial of n.

The hermite polynomials can be computed recursively by

$$H_0(t) = 1$$
$$H_1(t) = 2t$$
$$H_n(t) = 2t H_{n-1}(t) - 2(n-1) H_{n-2}(t). \qquad (2)$$

The set of functions $h_n(t, l)$ constitute a set of orthonormal basis functions referred to as AH functions [2]. They can be computed recursively using (1) and (2). The recursion relation thus obtained is

$$h_n(t) = \frac{1}{\sqrt{n}}[\sqrt{2}t h_{n-1}(t) - \sqrt{n-1} h_{n-2}(t)], \qquad n \geq 2. \qquad (3)$$

A signal $x(t)$ can be expanded into an AH series as

$$x(t) = \sum_{n=0}^{\infty} a_n h_n(t, l)$$
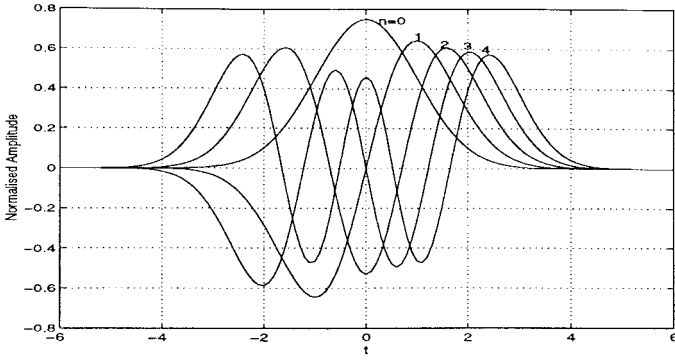$$= \sum_{n=0}^{\infty} \frac{a_n}{\sqrt{l}} h_n(t/l) \qquad (4)$$

Fig. 1.   Associate hermite functions of order zero to four.

where

$$h_n(t/l) = \sqrt{l}\,h_n(t, l). \tag{5}$$

Equation (5) is for notational convenience.

AH functions of order zero to four are plotted in Fig. 1. These functions provide finite support for all practical purposes and by varying the scaling factor l, the support provided by the expansion can be increased or decreased. The odd order functions are odd and the even order functions are even.

A signal with compact time support can be expanded as

$$x(t) = \sum_{n=0}^{N} \frac{a_n}{\sqrt{l_1}} h_n(t/l_1). \tag{6}$$

Using [3, p. 53, eqs. (14), (15)]

$$e^{-t^2/2} H_{2m}(t) = (-1)^m \sqrt{\frac{2}{\pi}} \int_0^{\infty} e^{-y^2/2} H_{2m}(y) \cos{(ty)}\,dy$$

$$e^{-t^2/2} H_{2m+1}(t)$$
$$= (-1)^m \sqrt{\frac{2}{\pi}} \int_0^{\infty} e^{-y^2/2} H_{2m+1}(y) \sin{(ty)}\,dy \tag{7}$$

it can be shown that the Fourier transform of $x(t)$ is given by

$$X(f) = \sum_{n=0}^{N/2} (-1)^n$$
$$\times \left[\frac{a_{2n}}{\sqrt{l_2}} h_{2n}(f/l_2) - j \frac{a_{2n+1}}{\sqrt{l_2}} h_{2n+1}(f/l_2) \right]$$
$$= \sum_{n=0}^{N} (-j)^n \frac{a_n}{\sqrt{l_2}} h_n(f/l_2) \tag{8}$$

where $l_2 = \frac{1}{2\pi l_1}$. (Here N is assumed to be even). Note that the real part of the transform $X(f)$ denoted by $X_R(f)$ is even and the imaginary part of $X(f)$ denoted by $X_I(f)$ is odd, as expected for real $x(t)$. Therefore, $X_R(f)$ can be represented by the even order AH functions and $X_I(f)$ can be represented by the odd order AH functions. It is important to note that the Hermite polynomials are the eigenfunctions of the Fourier transform operator.

To expand a causal signal $x(t)$ (i.e., $x(t) = 0$ for t), using the AH functions as a basis, we prefer to center the expansion

about $t = t_0$ rather than at $t = 0$; where t_0 is roughly around half the time support of $x(t)$. This is because the AH functions provide equal support on either side of the center of expansion. So centering the expansion about t_0 would require lesser terms in the expansion. Therefore, we now work with the transform pair $x(t + t_0) \leftrightarrow e^{j2\pi f t_0} X(f)$.

The choice of the scaling factor l_1 is crucial because it also affects l_2 and l_1 and l_2 decide the amount of support given by the AH functions to the time- and frequency-domain responses, respectively. given about 50–60% of initial time-domain data and an equal amount of low-frequency data with a proper choice of N (the order of the expansion) and l_1 (the scaling factor) it is possible to extrapolate in both domain.

In all the examples, a choice of l_1 is made such that the t axis and f axis are roughly scaled to $(-6, 6)$. The order of expansion (N) varies between 10–20 for different examples. The value of N can be decided by choosing a cutoff for the magnitude of the coefficients, i.e., discarding the ones which die out. Choosing an unnecessarily large N will introduce oscillations in the extrapolation region. The coefficients are obtained by solving a least-squares problem, using singular-value decomposition (SVD) [7]. Even though the matrix is ill conditioned, this is not a real problem as one is doing an approximation of the function.

A. Matrix Formulation

Let M_1 and M_2 be the number of time- and frequency-domain samples that are given. Then the matrix representation of time-domain data from (6) would be

$$\begin{bmatrix} h_0(t_1/l_1) & h_1(t_1/l_1) & \cdots & h_{N-1}(t_1/l_1) \\ h_0(t_2/l_1) & h_1(t_2/l_1) & \cdots & h_{N-1}(t_2/l_1) \\ \vdots & \vdots & \vdots & \vdots \\ h_0(t_{M_1}/l_1) & h_1(t_{M_1}/l_1) & \cdots & h_{N-1}(t_{M_1}/l_1) \end{bmatrix}_{M_1 \times N}$$
$$\cdot \begin{bmatrix} a_0 \\ a_1 \\ \vdots \\ a_{N-1} \end{bmatrix}_{N \times 1} = \sqrt{l_1} \begin{bmatrix} x(t_1) \\ x(t_2) \\ \vdots \\ x(t_{M_1}) \end{bmatrix}_{M_1 \times 1}. \tag{9}$$

The real part of $X(f)$ from (8) can be represented by the even order AH functions as (10), shown on the next page. The imaginary part of $X(f)$ from (8) can be represented by the odd order AH functions as (11), shown on the next page. Combining the three matrix equations we get (12), as shown at the bottom of the next page. The coefficients of the expansion are obtained by solving this matrix equation.

III. NUMERICAL EXAMPLES

In this section, five examples are presented to validate the above technique. A program to evaluate the currents on an arbitrarily shaped closed or open body using the electric field integral equation (EFIE) and triangular patching is used [5]. The rationale for doing this is that we are going to use the EFIE both in time [6] and in frequency domain [5]. We utilize the same surface patching scheme for both domains,

hence, eliminating some of the effects of discretization from this study. The triangular patching approximates the surface of the scatterer with a set of adjacent triangles. The current perpendicular to each nonboundary edge is an unknown to be solved for. The frequency-domain data was generated using the program described in [5].

Although the program can be used with an arbitrary excitation, we used a linearly polarized plane wave with a Gaussian profile in time. The excitation has the form

$$\mathbf{E}^{\text{inc}} = \mathbf{u_i} E_0 e^{-\frac{\gamma^2}{2}} \tag{13}$$

$$\begin{bmatrix} h_0(f_1/l_2) & -h_2(f_1/l_2) & \cdots & (-1)^{N/2-1}h_{N-1}(f_1/l_2) \\ h_0(f_2/l_2) & -h_2(f_2/l_2) & \cdots & (-1)^{N/2-1}h_{N-1}(f_2/l_2) \\ \vdots & \vdots & \vdots & \vdots \\ h_0(f_{M_2}/l_2) & -h_2(f_{M_2}/l_2) & \cdots & (-1)^{N/2-1}h_{N-1}(f_{M_2}/l_2) \end{bmatrix}_{M_2 \times N/2} \cdot \begin{bmatrix} a_0 \\ a_2 \\ \vdots \\ a_{N-2} \end{bmatrix}_{N/2 \times 1} = \sqrt{l_2} \begin{bmatrix} X_R(f_1) \\ X_R(f_2) \\ \vdots \\ X_R(f_{M_2}) \end{bmatrix}_{M_2 \times 1} \tag{10}$$

$$\begin{bmatrix} -h_1(f_1/l_2) & h_3(f_1/l_2) & \cdots & (-1)^{N/2}h_{N-2}(f_1/l_2) \\ -h_1(f_2/l_2) & h_3(f_2/l_2) & \cdots & (-1)^{N/2}h_{N-2}(f_2/l_2) \\ \vdots & \vdots & \vdots & \vdots \\ -h_1(f_{M_2}/l_2) & h_3(f_{M_2}/l_2) & \cdots & (-1)^{N/2}h_{N-2}(f_{M_2}/l_2) \end{bmatrix}_{M_2 \times N/2} \cdot \begin{bmatrix} a_1 \\ a_3 \\ \vdots \\ a_{N-1} \end{bmatrix}_{N/2 \times 1} = \sqrt{l_2} \begin{bmatrix} X_I(f_1) \\ X_I(f_2) \\ \vdots \\ X_I(f_{M_2}) \end{bmatrix}_{M_2 \times 1} \tag{11}$$

$$\begin{bmatrix} h_0(t_1/l_1) & h_1(t_1/l_1) & \cdots & h_{N-2}(t_1/l_1) & h_{N-1}(t_1/l_1) \\ \vdots & \vdots & \vdots & \vdots & \vdots \\ h_0(t_{M_1}/l_1) & h_1(t_{M_1}/l_1) & \cdots & h_{N-2}(t_{M_1}/l_1) & h_{N-1}(t_{M_1}/l_1) \\ h_0(f_1/l_2) & 0 & \cdots & 0 & (-1)^{N/2-1}h_{N-1}(f_1/l_2) \\ \vdots & \vdots & \vdots & \vdots & \vdots \\ h_0(f_{M_2}/l_2) & 0 & \cdots & 0 & (-1)^{N/2-1}h_{N-1}(f_{M_2}/l_2) \\ 0 & -h_1(f_1/l_2) & \cdots & (-1)^{N/2}h_{N-2}(f_1/l_2) & 0 \\ \vdots & \vdots & \vdots & \vdots & \vdots \\ 0 & -h_1(f_{M_2}/l_2) & \vdots & (-1)^{N/2}h_{N-2}(f_{M_2}/l_2) & 0 \end{bmatrix}_{(M_1+2M_2) \times N} \cdot \begin{bmatrix} a_1 \\ a_2 \\ \vdots \\ a_{N-1} \end{bmatrix}_{N \times 1} = \begin{bmatrix} \sqrt{l_1}x(t_1) \\ \vdots \\ \sqrt{l_1}x(t_{M_1}) \\ \sqrt{l_2}X_R(f_1) \\ \vdots \\ \sqrt{l_2}X_R(f_{M_2}) \\ \sqrt{l_2}X_I(f_1) \\ \vdots \\ \sqrt{l_2}X_I(f_{M_2}) \end{bmatrix}_{(M_1+2M_2) \times 1} \tag{12}$$
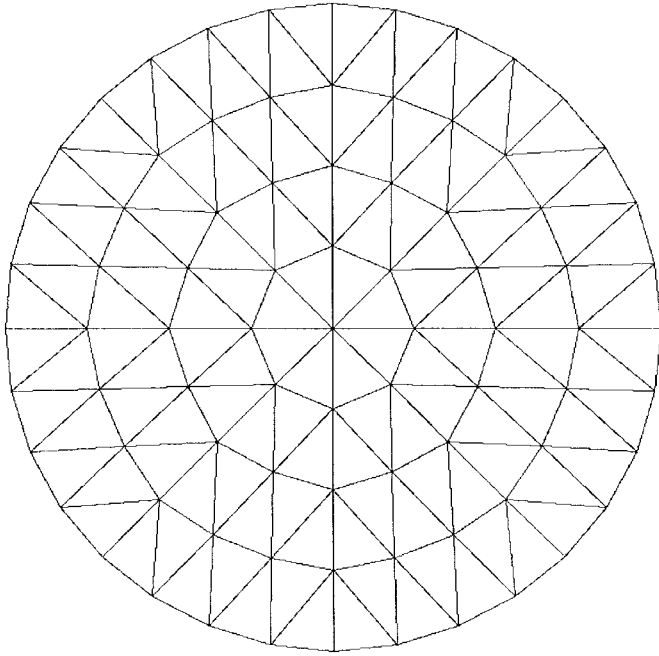
Fig. 2.   Triangle patching of a disk.

Fig. 3.   Time-domain response of the plate.

where

$$\gamma = \frac{(t - t_0 - \mathbf{r}.\mathbf{k})}{\sigma} \qquad (14)$$

$\mathbf{u_i}$ is the unit vector that defines the polarization of the incoming plane wave:

1) E_0 is the amplitude of the incoming wave;
2) σ controls the width of the pulse;
3) t_0 is a delay and is used so the pulse rises smoothly from zero for time $t < 0$ to its value at time t;
4) $\mathbf{r}$ is the position of an arbitrary point in space;
5) $\mathbf{k}$ is the unit wave vector defining the direction of arrival of the incident pulse.

To find the frequency response to the above Gaussian plane wave, the frequency response of the system is multiplied by the spectrum of the Gaussian plane wave. The spectrum is given by

$$F(j\omega) = \sqrt{2\pi}\sigma e^{-[(\omega\sigma)^2/2 + j\omega t_0]}, \qquad \omega = 2\pi f.$$

The bodies chosen are a plate, a disk, a sphere, a cube, and a cone-hemisphere combination. All bodies are assumed to be perfectly conducting. Fig. 2 shows an example of the triangulation scheme used. The figure shows a disk being approximated by 128 triangles and 208 edges. In all our computations, E_0 is chosen to be 377 V/m. The time step (Δt) is dictated by the discretization used in modeling the geometry of each example. The frequency step (Δf) is 2 MHz. In all examples, the extrapolated time-domain response is compared to the output of the marching-on-in-time (MoT) program [6]. And the extrapolated frequency-domain response is compared to the frequency response obtained from the MoM program [5]. In all the plots, *extrapolated signal* refers to the extrapolated response using AH expansions while *original signal* refers to the data obtained from the MoT or MoM program.
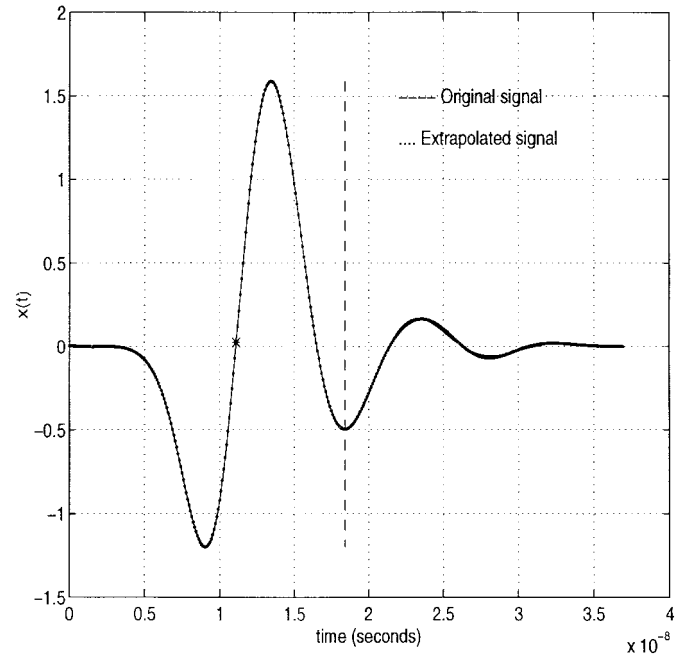
In these examples, causality is enforced only numerically by centering the approximation by the AH functions at $t = T_0$, somewhere in the middle of the time-domain data.

Example 1—Square Plate: In this example, we have a square plate of zero thickness and side 1m centered at the origin and in the xy plane. Eight divisions are made in the x direction and nine in the y direction. By joining the diagonals of each resulting rectangle, 144 triangular patches with 199 unknowns are obtained. The excitation arrives from the direction $\theta = 0$, $\phi = 0$; i.e., along the negative z direction. u_i is along the x axis. The time step used in the MoT program is $92.59ps$. In this example, $\sigma = 2ns$ and $t_0 = 10ns$.

Using the MoT algorithm, time-domain data is obtained from $t = 0$ to $t = 36.94ns$ (400 data points) and frequency-domain data is obtained from dc to $f = 298$ MHz (150 data points). Assume that only the first 200 time-data points (up to $t = 18.43ns$) and the first 60 frequency-data points (up to 118 MHz) are available. Solving for the matrix equation (12) using the available data, the time-domain response is extrapolated to 400 points (up to $t = 36.94ns$) and the frequency-domain response is extrapolated to 150 points (up to $f = 298$ MHz). Given a time-bandwidth product of 2.175, we extrapolate to a time bandwidth product of 11.

The order of expansion (N) was chosen to be 20 and the time-domain signal was centered about its first zero-crossing i.e., $t_0 = 11.11ns$ (denoted by "*" in the plots). A choice of l_2 was made such that the frequency range of available data (assuming around 50% is available), was mapped to $(-3, \ 3)$. This ensures that the time (with the time shift) and the frequency axes are roughly mapped in the range $(-6, \ 6)$.

From Fig. 3, it can be seen that the time-domain reconstruction is almost indistinguishable from the *actual* (MoT) data. The reconstruction in the frequency domain is also very good, as can be seen from Figs. 4 and 5.
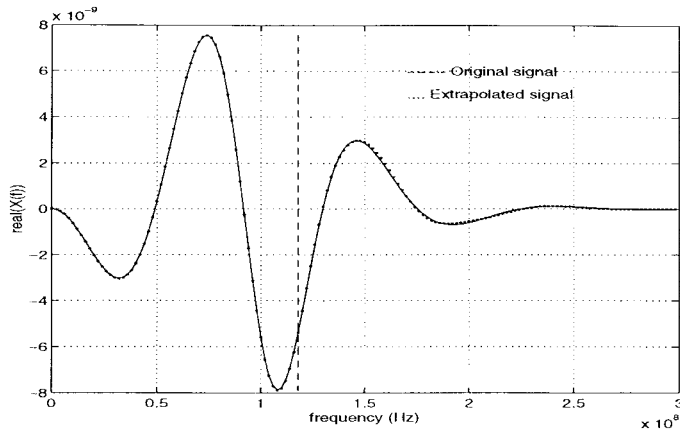
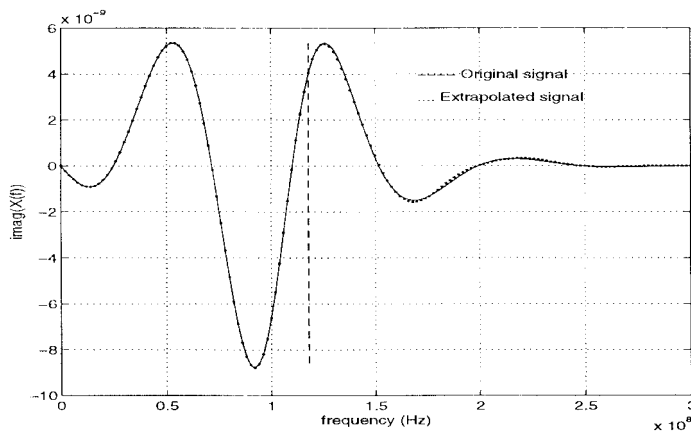Fig. 4. Frequency response of the plate; real part.

Fig. 5. Frequency response of the plate; imaginary part.

Fig. 6. Time-domain response of the disk.

Fig. 7. Frequency response of the disk; real part.

Example 2—Disk: A disk of radius 3 m of zero thickness lies in the xy plane and is centered at the origin. The triangulation uses 128 triangles resulting in 208 edges. Thirty-two of the edges are boundary edges, yielding 176 unknowns. The excitation arrives from $\theta = 0$, $\phi = 0$, i.e., along the negative z direction. $\mathbf{u_i}$ is along the x axis. Here $\sigma = 1ns$ and $t_0 = 10ns$. The time step used is $47.76ps$.

In this example, the MoT algorithm is used to obtain time-domain response from $t = 0$ to $t = 23.83ns$ (500 data points). And the frequency-domain response is obtained using the MoM program from dc to $f = 598$ MHz (300 data points). Assume that only the first 290 time-data points (up to $t = 13.80ns$) and the first 120 frequency-data points (up to $f = 238$ MHz) are available. Using this data, the time-domain response is extrapolated to 500 points (up to $t = 23.83ns$) and the frequency-domain response is extrapolated to 300 points (up to $f = 598$ MHz). Given a time-bandwidth product of 3.28, we extrapolate to a time-bandwidth product of 14.25.

The order of expansion (N) was chosen to be 16 and the time-domain signal was centered about its first zero crossing, i.e., $t_0 = 10.60ns$. A choice of l_2 such that the frequency range of available data was mapped to $(-3, 3)$. This ensures that the shifted t-axis and the f-axis are scaled in the range $(-6, 6)$.
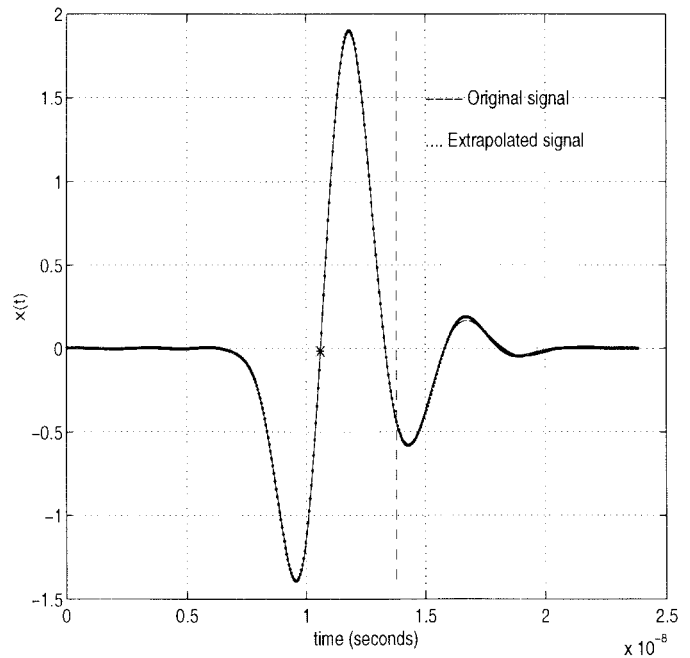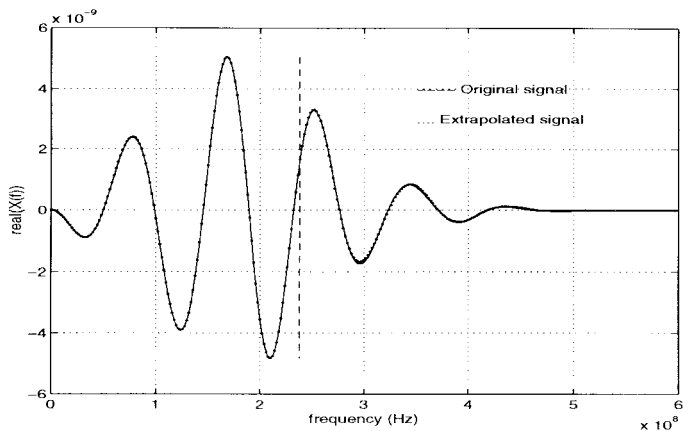
From Fig. 6, it can be seen that the time-domain reconstruction is almost identical to the *actual* (MoT) data. The reconstruction in the frequency domain agrees closely with *actual* MoM data, as can be seen from Figs. 7 and 8.

Example 3—Sphere: A sphere of radius 0.5m centered at the origin is considered next. The top half of the sphere ($\theta = 0$ to $\theta = \frac{\pi}{2}$) has six divisions in the θ direction. The first *ring* extends from $\theta = 0$ to $\theta = \frac{\pi}{16}$. The other five rings are equispaced in θ from $\theta = \frac{\pi}{16}$ to $\theta = \frac{\pi}{2}$. Each ring starting from the top has 6, 16, 20, 24, 28, and 32 triangular patches. The sphere is symmetric with respect to the xy plane. This scheme is chosen so all triangles are as close to equilateral as possible. If the ϕ direction were also divided uniformly, the triangles would be skewed. Also, this scheme allows us to evaluate the current at the point $(-0.5, 0.0, 0.0)$. The excitation arrives along $\theta = \frac{\pi}{2}$, $\phi = \pi$, i.e., along the x direction. $\mathbf{u_i}$ is along the z axis. In this example, $\sigma = 3ns$ and $t_0 = 22ns$. The time step used in the MoT program is $0.199\,43ns$.
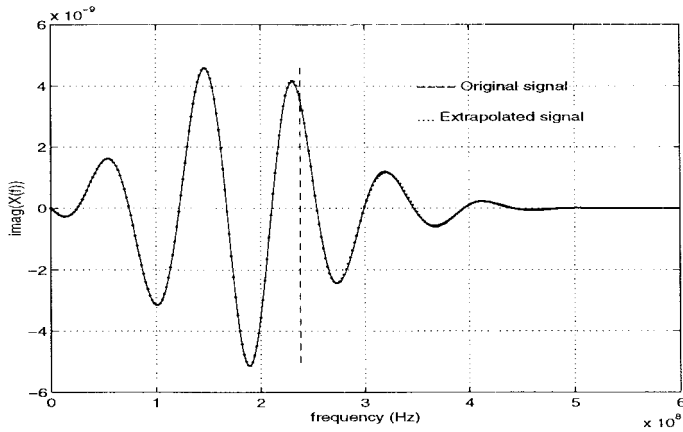
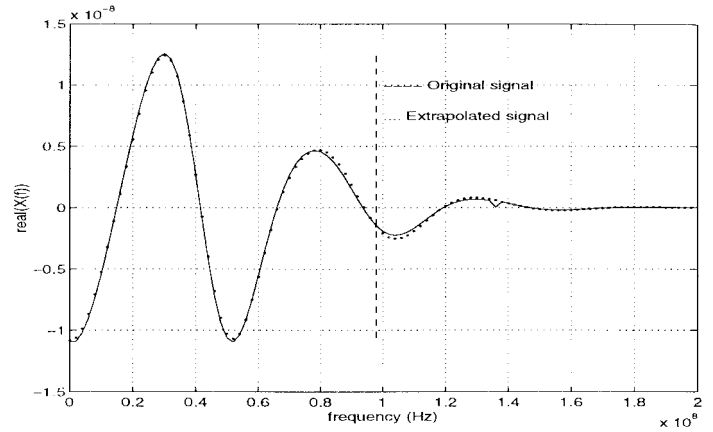Fig. 8. Frequency response of the disk; imaginary part.
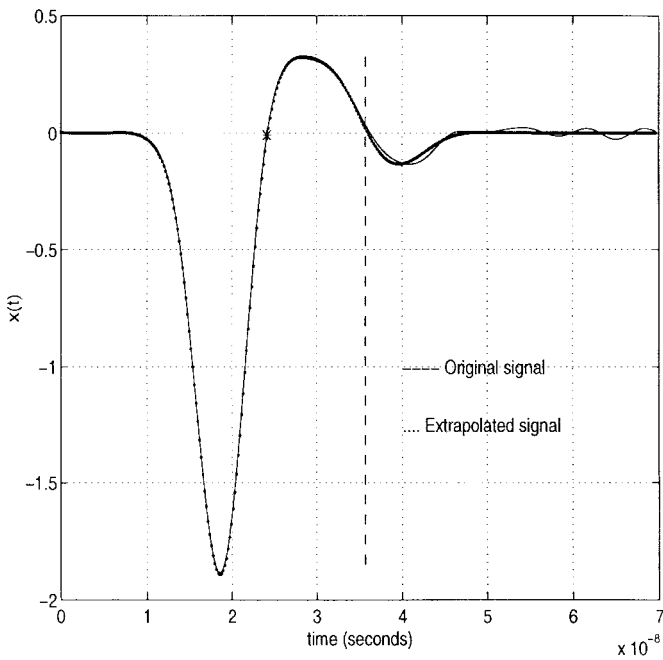

Fig. 10. Frequency response of the sphere; real part.

Fig. 9. Time-domain response of the sphere.

Fig. 11. Frequency response of the sphere; imaginary part.

The time-domain response is obtained using the MoT algorithm from $t = 0$ to $t = 69.60ns$ (350 data points) and the frequency-domain response is obtained using the MoM program from dc to $f = 198$ MHz (100 data points). Using the first 180 data points (up to $t = 35.7ns$) and the first 50 f-data points (up to $f = 98$ MHz), the time-domain response is extrapolated to 350 points (up to $t = 69.6ns$) and the frequency-domain response is extrapolated to 300 points (up to $f = 198$ MHz). In this example, given a time bandwidth product of 3.45, we extrapolate to a time bandwidth product of 13.78.

The order of the expansion (N) was chosen to be 15 and the time-domain signal is centered about its first zero-crossing i.e., $t_0 = 24.13ns$. l_2 is chosen such that the frequency range of the available data is mapped to $(-3, 3)$. This ensures that the shifted t axis and the f axis are mapped in the range $(-6, 6)$.

The time-domain response reconstruction is agreeable to the *actual* MoT data, as seen in Fig. 9. From Figs. 10 and 11 it
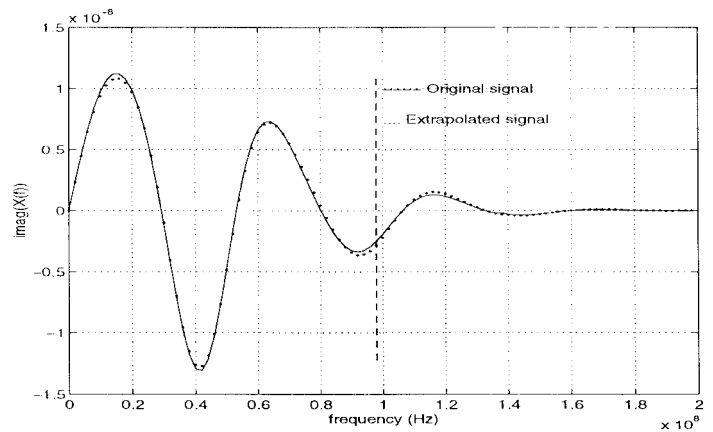
can be seen that the *real* and *imag* parts also have reasonably good reconstruction using the AH expansions.

Example 4—Cube: In this example, a cube of side 1 m centered at the origin with its faces lined up along the three coordinate axis is considered. The faces at $x = 0.5$m and $x = -0.5$m have five divisions in the y and z direction. All other faces have four divisions in one direction and five in the other. This allows us to find the current at the center of the top face. The excitation arrives from the direction $\theta = 0$, $\phi = 0$, i.e., along the $-z$ direction. $\mathbf{u_i}$ is along the x axis. In this example, $\sigma = 2.357ns$ and $t_0 = 20ns$. The time step chosen for the MoT program is $0.157\,13ns$.

The time-domain response of the cube, is calculated using the MoT algorithm from $t = 0$ to $t = 46.98ns$ (300 data points). And the frequency-domain response is calculated with the MoM program from dc to $f = 298$ MHz (150 data points). Assuming that only the first 180 t-data points (up to $t = 28.93ns$) and the first 60 f-data points (up to $f = 118$ MHz), the time-domain response was extrapolated to 300 data points (up to $t = 46.98ns$) and the frequency-domain response is extrapolated to 150 points (up to $f = 298$ MHz). Given a time-bandwidth product of 3.41, we extrapolate to a time-bandwidth of ten.

N was chosen to be 15 and again the t-domain response was centered about its first zero-crossing, i.e., $t_0 = 21.68ns$. l_2 is such that the frequency range of the available data is
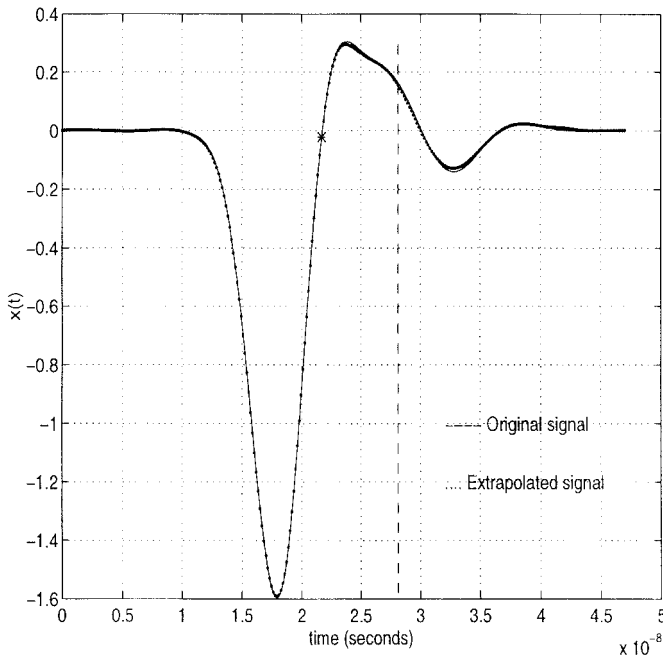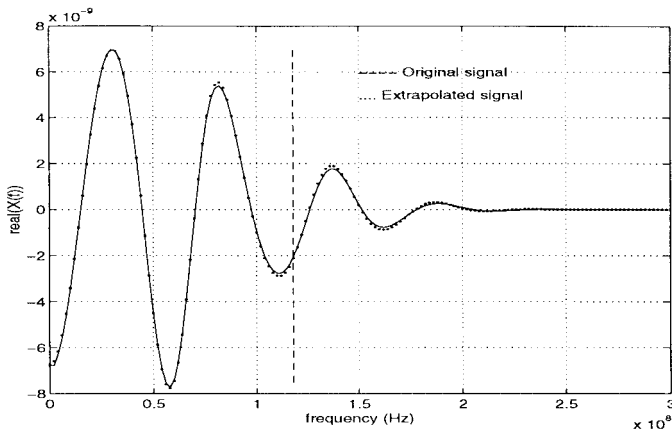
Fig. 12.   Time-domain response of the cube.
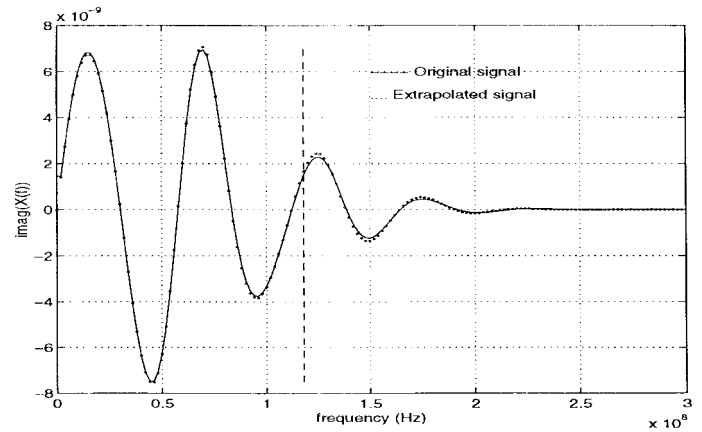

Fig. 14.   Frequency response of the cube; imaginary part.

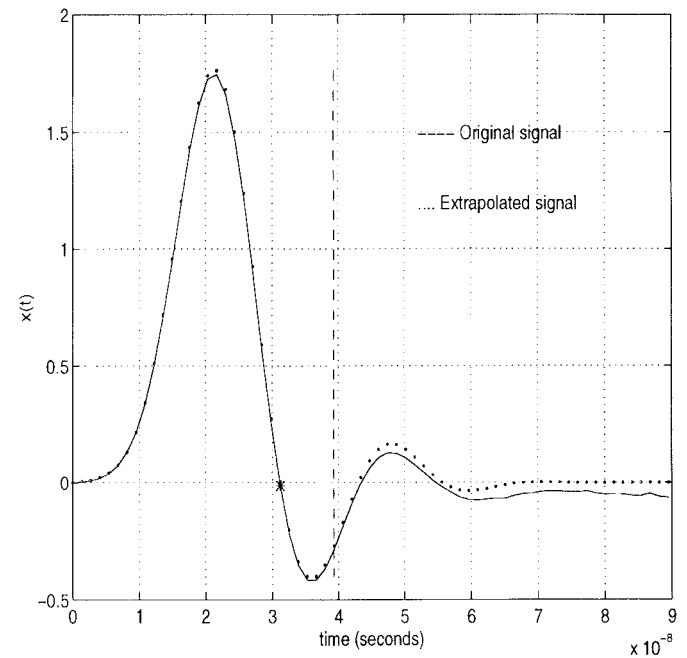Fig. 13.   Frequency response of the cube; real part.

Fig. 15.   Time-domain response of the cone.

mapped to $(-3, \ 3)$. This ensures that the shifted t axis and the f axis are mapped in the range $(-6, \ 6)$.

From Fig. 12, the time-domain response can be seen to closely agree with the *actual* MoT data. The frequency-domain reconstruction is agreeable in comparison to the *actual* MoM data as can be seen from Figs. 13 and 14.

Example 5–Cone-Hemisphere: In this example, we have a combination of a cone and hemisphere with the hemisphere attached to the base of the cone and their center at the origin. The base of the cone and hemisphere have a radius of 1m and the height of the cone is 2m. The central axis of the combination lies in the z direction.

The triangular patch approximation for the cone has six divisions in the z direction. The planes defining the "rings" are at $z = 2.0$, $z = 1.75$, $z = 1.4$, $z = 1.05$, $z = 0.7$, $z = 0.35$ and $z = 0$. Each ring starting from the top has 7, 16, 20, 24, 28, and 32 triangles, respectively. The hemisphere has three divisions in the θ direction. The "rings" extend from $\theta = \pi$

to $\theta = \frac{2\pi}{3}$, $\theta = \frac{5\pi}{6}$ to $\theta = \frac{2\pi}{3}$, and $\theta = \frac{2\pi}{3}$ to $\theta = \frac{\pi}{2}$. Each ring starting from the bottom has 13, 28, and 32 triangular patches, respectively. Such a triangulation scheme allows for the current at the point $(-0.1, \ 0.0, \ 0.0)$ to be evaluated.

The excitation arrives from $\theta = \frac{\pi}{2}$, $\phi = \pi$, i.e., along the x direction. $\mathbf{u_i}$ is along the z axis. In this example, $\sigma = 6ns$ and $t_0 = 25ns$. The time step used is $90.39ps$. The frequency step used is 2 MHz.

The time-domain response is calculated using the MoT program from $t = 0$ to $t = 90.30ns$ (67 points using every 15th point in the time-domain data). This was done so that in the least-squares analysis, both the t-domain and f-domain data have the same weightage and the frequency-domain response is calculated using the MoM algorithm from dc to $f = 98$ MHz (50 data points). Using the first 30 t-data points (up to $t = 40.59ns$) and the first 25 f-data points (up to $f = 48$ MHz), the time-domain response is extrapolated to 67 points (up to $t = 90.30ns$) and the frequency-domain
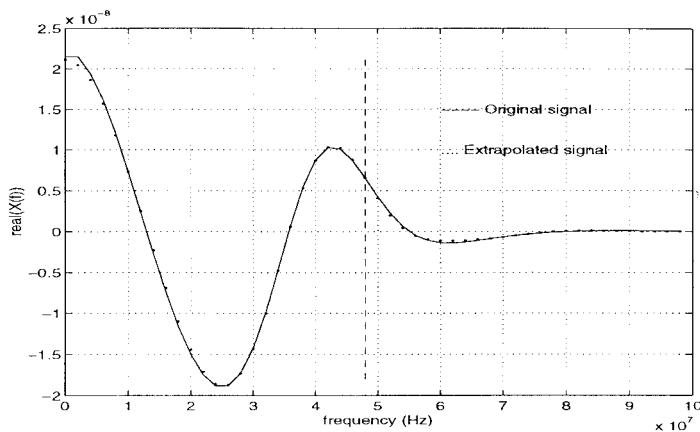
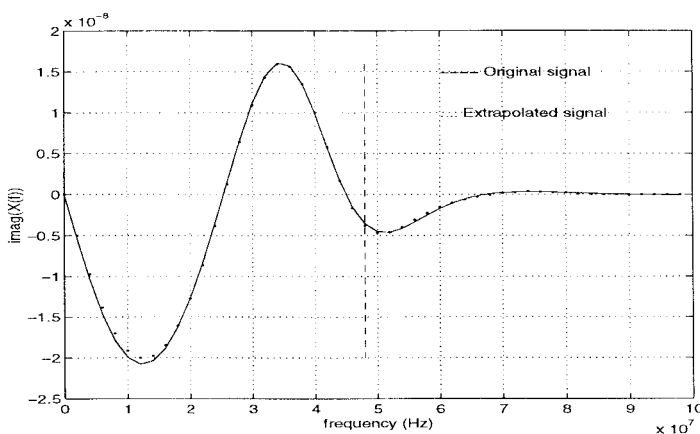Fig. 16. Frequency response of the cone; real part.

Fig. 17. Frequency response of the cone; imaginary part.

response is obtained up to 50 points (up to $f = 98$ MHz). In this example, starting with a time-bandwidth product of 1.95, we extrapolate to a time-bandwidth product of 8.85.

N was chosen to be 12 and the time-domain response was again centered about its first zero crossing, i.e., $t_0 = 34ns$ and l_2 is chosen as usual to map the frequency range of available data to $(-3, 3)$. This ensures that the shifted t axis and the f axis is mapped in the range $(-6, 6)$.

From Fig. 15, the extrapolated time-domain response is agreeable with the MoT data. The frequency-domain responses are seen to agree reasonably well with the *actual* MoM data, as can be seen from Figs. 16 and 17.

IV. CONCLUSIONS

This paper deals with the problem of extrapolation using both time- and frequency-domain data. We have presented a new mathematical technique to perform simultaneous extrapolation in both domains using the AH expansions. The computation involved is minimal because we require only early-time and low-frequency information. This, coupled with the fact that expansions of orders less than 20 give good representation of the signals in both domains ensures that this method is computationally very efficient.

In this paper, we have applied this technique to the problem of extrapolating the current on a scatterer being excited by a uniform plane wave. Five scatterers were considered—a plate, disk, sphere, cube, and cone. Using early-time and low-frequency data, we have demonstrated good extrapolation in both domains. It appears from the limited examples that one can extrapolate the time-bandwidth product of responses typically by a factor of three to five. Currently, work is underway to determine the limiting factors of this methodology and how far the data can be extrapolated without significant errors. The minimum time-bandwidth necessary to carry out extrapolation is also being investigated.

REFERENCES

[1] R. S. Adve, T. K. Sarkar, and O. M. Pereira-Filho, "Extrapolation of time-domain responses from three-dimensional conducting objects utilizing the matrix pencil technique," *Trans. Antennas Propagat.*, vol. 45, pp. 147–156, Jan. 1997.
[2] R. L. Conte Loredana, R. Merletti, and G. V. Sandri, "Hermite expansions of compact support signals: Applications to myoelectric signals," *IEEE Trans. Biomed. Eng.*, vol. 41, pp. 1147–1159, Dec. 1994.
[3] A. D. Poularikas, *The Transforms and Applications Handbook.* New York: IEEE Press, 1996.
[4] S. Narayana, T. K. Sarkar, and R. S. Adve, "A comparison of two techniques for the interpolation/extrapolation of frequency-domain responses," *Digital Signal Processing*, vol. 6, no. 1, pp. 51–67, Jan. 1996.
[5] S. M. Rao, Electromagnetic scattering and radiation of arbitrarily shaped surfaces by triangular patch modeling, Ph.D. dissertation, Univ. Mississippi, 1978.
[6] D. A. Vechinski, Direct time-domain analysis of arbitrarily shaped conducting or dielectric structures using patch modeling techniques, Ph.D. dissertation, Auburn University, AL, 1992.
[7] G. H. Golub and C. F. Van Loan, *Matrix Computations.* Baltimore, MD: Johns Hopkins Univ. Press, 1991.

Murli Mohan Rao, photograph and biography not available at the time of publication.

Tapan K. Sarkar (S'69–M'76–SM'81–F'92), for a photograph and biography, see p. 493 of the April 1998 issue of this TRANSACTIONS.

Tricha Anjali, photograph and biography not available at the time of publication.

Raviraj S. Adve, for photograph and biography, see p. 493 of the April 1998 issue of this TRANSACTIONS.